Bulletin of Mathematical Biology (2008) 70: 992–1012
DOI 10.1007/s11538-007-9287-9

ORIGINAL ARTICLE

Reoxygenation and Split-Dose Response to Radiation in a Tumour Model with Krogh-Type Vascular Geometry

A. Bertuzzi[a,*], A. Fasano[b], A. Gandolfi[a], C. Sinisgalli[a]

[a] *Istituto di Analisi dei Sistemi ed Informatica del CNR, Viale Manzoni 30, 00185 Roma, Italy*
[b] *Dipartimento di Matematica "U. Dini", Università degli Studi di Firenze, Viale Morgagni 67/A, 50134 Firenze, Italy*

Received: 9 March 2007 / Accepted: 29 October 2007 / Published online: 13 February 2008

Abstract After a single dose of radiation, transient changes caused by cell death are likely to occur in the oxygenation of surviving cells. Since cell radiosensitivity increases with oxygen concentration, reoxygenation is expected to increase the sensitivity of the cell population to a successive irradiation. In previous papers we proposed a model of the response to treatment of tumour cords (cylindrical arrangements of tumour cells growing around a blood vessel of the tumour). The model included the motion of cells and oxygen diffusion and consumption. By assuming parallel and regularly spaced tumour vessels, as in the Krogh model of microcirculation, we extend our previous model to account for the action of irradiation and the damage repair process, and we study the time course of the oxygenation and the cellular response. By means of simulations of the response to a dose split in two equal fractions, we investigate the dependence of tumour response on the time interval between the fractions and on the main parameters of the system. The influence of reoxygenation on a therapeutic index that compares the effect of a split dose on the tumour and on the normal tissue is also investigated.

Keywords Radiotherapy · Reoxygenation · Dose splitting · Krogh model · Tumour cords

1. Introduction

After the delivery of a dose of radiation, important changes that will influence the effect of a subsequent dose occur in the irradiated tumour cell population. The most important processes occurring after irradiation are denoted as the 4R's of radiotherapy: repair of radiation damage, redistribution of cells among the cell-cycle phases, reoxygenation, and repopulation due to regrowth of surviving cells (Wong and Hill, 1998). Redistribution and reoxygenation are expected to recover and, respectively, to transiently increase

*Corresponding author.
E-mail addresses: bertuzzi@iasi.cnr.it (A. Bertuzzi), fasano@math.unifi.it (A. Fasano), gandolfi@iasi.cnr.it (A. Gandolfi), sinisgalli@iasi.cnr.it (C. Sinisgalli).

the pretreatment radiosensitivity (Wong and Hill, 1998). A simple representation of this resensitization that contrasts the effects of damage repair and repopulation has been incorporated in an extension of the so-called LQ model (Thames, 1985) for the response to two dose fractions (Brenner et al., 1995).

We will focus mainly on cell reoxygenation (Vaupel et al., 1984; Goda et al., 1995; Crokart et al., 2005), and will model this phenomenon in the framework of an idealized representation of tumour vascularization, i.e. by adopting the geometry of the Krogh model of microcirculation (Krogh, 1919; Popel, 1989). In this model, the vascular network is assumed to be an array of parallel and regularly spaced vessels, so that the tissue can be partitioned into identical cylinders, each surrounding a central vessel (Krogh cylinders). Observations of experimental tumours suggest that the increased oxygenation level that occurs after irradiation can be caused by an increase in blood perfusion (Sonveaux et al., 2002; Crokart et al., 2005) and/or by a decrease in the oxygen consumption by the tissue (Crokart et al., 2005; Ljungkvist et al., 2006). In our theoretical study, we restrict ourselves to assuming that the decrease in oxygen consumption due to treatment-induced cell death is the only cause of reoxygenation.

In previous papers (Bertuzzi et al., 2003, 2004, 2007) we proposed a mathematical model of the response to single-dose treatments of cylindrical arrangements of tumour cells growing around blood vessels of the tumour (tumour cords). That model included the spatial distribution of cells, cell motion, and oxygen diffusion and consumption. To describe the response to irradiation, the model has been extended in the present paper by including the kinetics of the repair/misrepair process of radiation damage. By means of this model, we have investigated the time course of oxygenation after a single dose and the influence of reoxygenation on the response to two impulsive irradiations separated by a time interval (split-dose response). Experimental evaluations of the split-dose response have been reported, e.g. by Belli et al. (1967), Jostes et al. (1985), O'Hara et al. (1998).

The paper has the following outline. In Section 2, we illustrate the general modeling assumptions concerning the kinetics of radiation damage production and repair. In Section 3, the mathematical model for the tumour cord response is formulated. Section 4 reports the results of model simulation of the single-dose response, and of the split-dose response compared with the response to the single undivided dose. Still in Section 4, the influence of reoxygenation on a therapeutic index, which compares the effect of a split dose on the tumour and on the normal tissue, is investigated. Some concluding remarks are given in Section 5.

2. Kinetics of damage production and repair

Radiation produces a variety of lesions in the cell, with some of the most important repair and misrepair reactions involving the double strand breaks (DSB) of DNA (Sachs et al., 1997). These lesions induce a lethal damage in a fraction of cells that lose the capacity of continuous proliferation and will die at a subsequent time (clonogenically dead cells). Thus, after irradiation, the living tumour cell population will be composed by a subpopulation of viable cells and a subpopulation of live but lethally damaged, clonogenically dead cells. We assume that before irradiation all cells are viable.

Several mathematical models have been proposed to describe the kinetics of radiation damage production and repair (Sachs et al., 1997). We have adopted the model originally

proposed by Curtis (1986) and subsequently by Hlatky et al. (1994). In this model two pathways of lethal damage production are considered: the direct action of radiation and the binary misrepair of the DSBs. Denoting by N the number of viable cells in a homogeneous population and by U the mean number of DNA double strand breaks per cell, the model can be written as

$$\frac{dN}{dt} = -\left[\alpha \dot{D} + \frac{1}{2} k U^2\right] N, \tag{1}$$

$$\frac{dU}{dt} = \delta \dot{D} - \omega U - 2 k U^2, \tag{2}$$

where $\dot{D}$ is the dose rate, α represents the direct lethal action of radiation due to non-repairable lesions, δ is a coefficient that represents the production of (potentially) repairable DSBs, ω is the rate constant of DSB repair, and k is the rate constant of binary DSB misrepair. As shown by Eq. (2), in addition to the correct repair process that occurs with rate constant ω, DSBs may undergo misrepair due to the encounter of two DNA fragments belonging to different chromosomes. For each binary misrepair, which occurs with rate kU^2, two DSBs are removed. On average, one-half of these misrepairs is lethal to the cell because of the formation of a dicentric chromosome plus an acentric fragment. The proliferation of viable cells is disregarded in Eq. (1).

The above kinetic model explains the empirical dose-response relationship known as the linear quadratic (LQ) model (Thames, 1985; Bristow and Hill, 1998). By identifying the surviving fraction after a single impulsive dose D at the time $t = 0$ as the ratio $S = N(\infty)/N(0^-)$, the model (1), (2) predicts for S the following approximate expression (Hlatky et al., 1994, see also Appendix A):

$$S = \exp\left[-\alpha D - \beta D^2\right], \tag{3}$$

where the coefficient β is given by

$$\beta = \frac{\delta^2 k}{4\omega}. \tag{4}$$

Equation (4) shows that the quadratic dependence on the dose is related to the process of binary misrepair. If the radiation dose is split into two half-doses delivered with a time interval T, the surviving fraction, according to model (1), (2), becomes

$$S = \exp\left[-\alpha D - \beta\left(1 + \mathrm{e}^{-\omega T}\right)\frac{D^2}{2}\right]. \tag{5}$$

The survival after the split-dose delivery, according to the above equation, is larger than the survival after the undivided dose, because part of the damage caused by the first dose is repaired in the time interval between the two fractions.

It is well known that the radiosensitivity parameters of a cell population, α and β, depend on the oxygenation of the cells (Chapman et al., 1974; Wouters and Brown, 1997). The increase of oxygenation observed in tumours after a dose of radiation and the regrowth of surviving cells are not accounted for in the expression (5). The effects of these phenomena will be studied by the tumour model illustrated in the following sections.

3. Tumour cord model

We model the tumour vascular network according to the Krogh model of microcirculation. This model is a highly idealized representation when dealing with tumours (Secomb et al., 1993), because it is well known that tumour vasculature has a very irregular structure. However, this assumption allows to develop a relatively simple analytical study, and similar assumptions on the structure of vascular network have indeed been adopted by Kocher and Treuer (1995), Kocher et al. (2000), and Alarcón et al. (2003).

Therefore, the tumour tissue will be partitioned into circular cylinders of radius B around straight central blood vessels, with B the half-distance between adjacent vessels (see Fig. 1A). We assume that vessels move solidly with the tumour tissue always keeping their symmetry, so their distance will increase during tumour expansion and will decrease during tumour regression. In view of this assumption, we can take that there is no exchange of matter across the surfaces of radius B and each cylinder of cells can be studied independently of any other. We denote by r the radial distance from the axis and by r_0 the radius of the central vessel. If the distance among vessels exceeds a limiting value, necrosis will appear in the regions more distant from the vessels, and isolated cylindrical regions of viable cells of radius ρ_N will form (see Fig. 1B). These cellular arrangements are called tumour cords (Tannock, 1968; Hirst and Denekamp, 1979; Moore et al., 1985). Necrotic regions may be observed in tumours at an advanced stage of growth. In the following, we will refer to tumour cords also for the Krogh cylinders of tumour cells in the absence of necrosis.

In a cord we will distinguish viable proliferating (P) and quiescent (Q) cells, lethally damaged cells, and dead cells. Under the continuum hypothesis, we can consider the volume fractions occupied locally by these components, denoting these fractions as v_P,

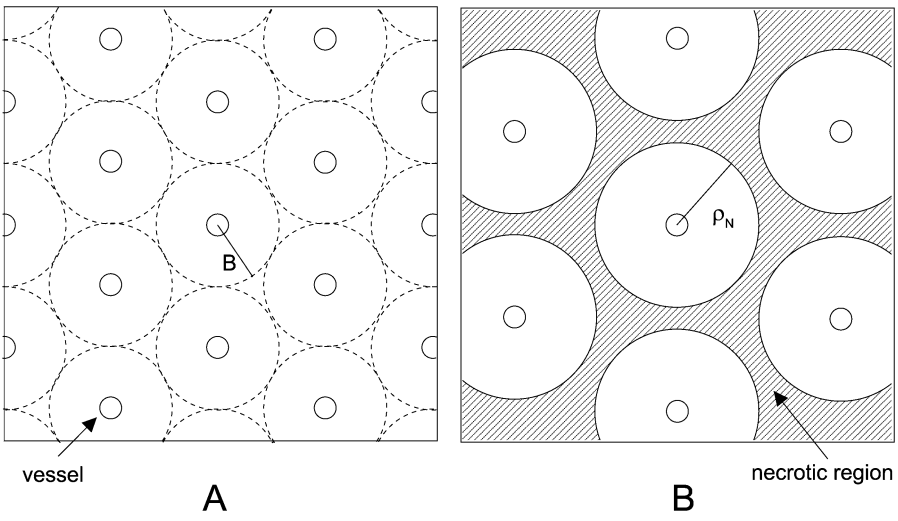

Fig. 1 Scheme of the assumed vascular geometry. Panel A: vessels close enough to sustain the viability of all surrounding cells. Panel B: increased distance among vessels causes distal necrosis. Symbols are explained in the text.

ν_Q, $\nu^\dagger$ and, respectively, ν_N. We assume that radiation treatment does not affect the tumour vasculature in the time horizon considered.

The main assumptions of the model are summarized as follows. (i) The cord has cylindrical symmetry, and all the model variables are independent of the axial coordinate. Therefore, all the model variables are functions of r and t. (ii) The velocity of the cellular component is radially directed and is the same for both live and dead cells. This common velocity is denoted as $u(r,t)$. (iii) Cells can undergo transitions between the proliferating and the quiescent state, and the transition rates are regulated by the oxygen concentration $\sigma(r,t)$. (iv) We assume that cells die instantaneously when σ falls to a critical value σ_N. (v) Only impulsive irradiations will be considered. According to the model by Hlatky et al. (1994), a fraction of lethally damaged cells is formed instantly after a radiation pulse because of the direct action of radiation. Subsequently, lethally damaged cells will be formed with rates dependent on the misrepair process (see Fig. 2A). The radiosensitivity parameters α and β are increasing functions of σ, possibly different for P and Q cells. (vi) Lethally damaged cells cease to progress across the cell cycle and die with rate constant μ. (vii) Dead cells are degraded to a fluid waste with rate μ_N and are drained away by the flow of extracellular fluid along the axial direction of the cord. (viii) The total volume fraction of cells is constant in space and time. In other words, it is assumed that live

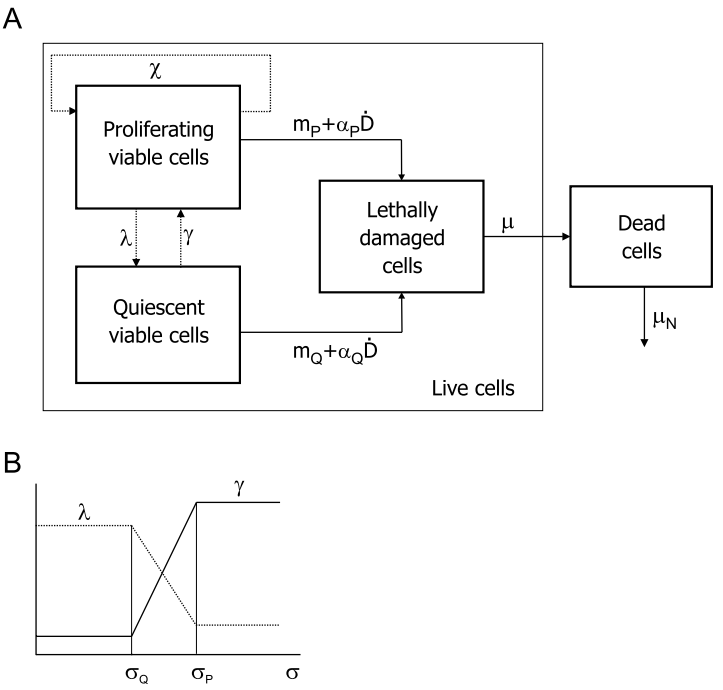

Fig. 2 Panel A: block diagram illustrating the cell subpopulations included in the model. The meaning of the symbols is explained in the text; the terms $\alpha_P \dot{D}$ and $\alpha_Q \dot{D}$ represent the direct damaging action of radiation. Panel B: profile of the functions $\lambda(\sigma)$ and $\gamma(\sigma)$ that govern the transitions from proliferation into quiescence and from quiescence to proliferation.

and dead cells possess a uniform spatial arrangement, which is quickly recovered after any perturbation caused by cell proliferation and degradation of dead cells. Experimental measurements support assumption (viii) in the absence of treatment, since data from tumour cords show small changes in the cell density with the radial distance (Moore et al., 1984, 1985). However, the hypothesis that total cell volume fraction is constant is an oversimplification in the transient that follows a treatment, when an increased volume fraction of extracellular fluid has been observed (Zhao et al., 1996). This hypothesis might be relaxed by adopting the two-fluid model of tumour tissue (Byrne and Preziosi, 2003).

Assuming that all the components have equal mass density, the mass balance yields the following conservation equations for the volume fractions:

$$\frac{\partial \nu_P}{\partial t} + \frac{1}{r}\frac{\partial}{\partial r}(ru\nu_P) = \chi \nu_P + \gamma(\sigma)\nu_Q - \lambda(\sigma)\nu_P - m_P(r,t)\nu_P, \tag{6}$$

$$\frac{\partial \nu_Q}{\partial t} + \frac{1}{r}\frac{\partial}{\partial r}(ru\nu_Q) = -\gamma(\sigma)\nu_Q + \lambda(\sigma)\nu_P - m_Q(r,t)\nu_Q, \tag{7}$$

$$\frac{\partial \nu^\dagger}{\partial t} + \frac{1}{r}\frac{\partial}{\partial r}(ru\nu^\dagger) = m_P(r,t)\nu_P + m_Q(r,t)\nu_Q - \mu\nu^\dagger, \tag{8}$$

$$\frac{\partial \nu_N}{\partial t} + \frac{1}{r}\frac{\partial}{\partial r}(ru\nu_N) = \mu\nu^\dagger - \mu_N\nu_N, \tag{9}$$

where $\lambda(\sigma)$ and $\gamma(\sigma)$ denote the transition rate from proliferation into quiescence and, respectively, the transition rate from quiescence into proliferation. The rates m_P and m_Q represent the production of lethal damage due to the misrepair process. Since from assumption (viii) the sum $\nu_P + \nu_Q + \nu^\dagger + \nu_N = \nu^\star$ is constant, the velocity field $u(r,t)$ satisfies the equation

$$\nu^\star \frac{1}{r}\frac{\partial}{\partial r}(ru) = \chi\nu_P - \mu_N\nu_N, \qquad u(r_0,t) = 0.$$

The rates λ and γ will be taken as a nonincreasing and, respectively, a nondecreasing function of σ. In particular, we assign two threshold values for σ, $\sigma_P > \sigma_Q$, and we assume: $\lambda = \lambda_{\max}$ and $\gamma = \gamma_{\min}$ for $\sigma \le \sigma_Q$, $\lambda = \lambda_{\min}$ and $\gamma = \gamma_{\max}$ for $\sigma \ge \sigma_P$, with $\lambda_{\max} > \lambda_{\min} \ge 0$ and $\gamma_{\max} > \gamma_{\min} \ge 0$. $\lambda(\sigma)$ decreases linearly and $\gamma(\sigma)$ increases linearly in the interval (σ_Q, σ_P) (see Fig. 2B). Although experimental data suggest a reduction in the rate of progression across the cell cycle as the nutrient concentration decreases, for simplicity we take a constant proliferation rate χ independent of σ.

In view of the model by Hlatky et al. (1994) for the kinetics of DSB repair/misrepair, for the rates m_P and m_Q we will assume

$$m_P(r,t) = \frac{1}{2}kX_P^2(r,t), \qquad m_Q(r,t) = \frac{1}{2}kX_Q^2(r,t), \tag{10}$$

where $X_P(r,t)$ and $X_Q(r,t)$ denote the mean number of DSBs in an "equivalent" P cell and, respectively, Q cell at the position r at time t (see Appendix B). These quantities, as derived in the Appendix, satisfy the following equations:

$$\frac{\partial X_P}{\partial t} + u\frac{\partial X_P}{\partial r} = -\omega X_P - 2kX_P^2, \tag{11}$$

$$\frac{\partial X_Q}{\partial t} + u\frac{\partial X_Q}{\partial r} = -\omega X_Q - 2kX_Q^2. \tag{12}$$

The rate constants ω and k are taken to be independent of the oxygen concentration.

Because we are considering only impulsive irradiation, the direct action of radiation (the term $\alpha\dot{D}$ in Eq. (1)) and the production of repairable DSBs ($\delta\dot{D}$ in Eq. (2)) will be represented in the initial conditions. The DSB production will occur with sensitivity coefficients $\delta_P(\sigma(r,t))$ and $\delta_Q(\sigma(r,t))$. If a sequence of impulsive irradiations is given with dose D_i at time t_i, $i = 1, 2, \ldots$, $t_1 = 0$, we have the following initial conditions for Eqs. (6)–(8), (11), (12):

$$\begin{aligned}
&v_P\big(r,t_i^+\big) = \exp\big[-\alpha_P\big(\sigma(r,t_i^-)\big)D_i\big]v_P(r,t_i^-),\\
&v_Q\big(r,t_i^+\big) = \exp\big[-\alpha_Q\big(\sigma(r,t_i^-)\big)D_i\big]v_Q(r,t_i^-),\\
&v^\dagger\big(r,t_i^+\big) = \big(1-\exp\big[-\alpha_P\big(\sigma(r,t_i^-)\big)D_i\big]\big)v_P(r,t_i^-)\\
&\qquad\qquad + \big(1-\exp\big[-\alpha_Q\big(\sigma(r,t_i^-)\big)D_i\big]\big)v_Q(r,t_i^-) + v^\dagger(r,t_i^-),\\
&X_P\big(r,t_i^+\big) = \delta_P\big(\sigma(r,t_i^-)\big)D_i + X_P(r,t_i^-),\\
&X_Q\big(r,t_i^+\big) = \delta_Q\big(\sigma(r,t_i^-)\big)D_i + X_Q(r,t_i^-).
\end{aligned}$$

The dependence on the oxygen concentration of the radiosensitivity parameters of LQ model, α and β, was expressed as (Wouters and Brown, 1997)

$$\alpha_P(\sigma) = \alpha_M^P\psi_\alpha(\sigma), \qquad \alpha_Q(\sigma) = \alpha_M^Q\psi_\alpha(\sigma), \tag{13}$$

$$\beta_P(\sigma) = \beta_M^P\psi_\beta^2(\sigma), \qquad \beta_Q(\sigma) = \beta_M^Q\psi_\beta^2(\sigma). \tag{14}$$

According to (4), $\delta_P(\sigma)$ and $\delta_Q(\sigma)$ are thus given by

$$\delta_P(\sigma) = \sqrt{\frac{4\omega}{k}\beta_M^P}\,\psi_\beta(\sigma), \qquad \delta_Q(\sigma) = \sqrt{\frac{4\omega}{k}\beta_M^Q}\,\psi_\beta(\sigma).$$

At $t = 0^-$, we have $v_P(r,0^-) = v_{P_0}(r)$, $v_Q(r,0^-) = v_{Q_0}(r)$, and all the other state variables are zero. Note that, since $u(r_0,t) = 0$, no boundary conditions are required for Eqs. (6)–(9).

Concerning the equation for the oxygen concentration, σ, we recall that diffusion is the dominant transport mechanism for oxygen and that it occurs in a quasi-stationary regime (Tannock, 1968). Assuming for simplicity that the oxygen consumption rate is the same for all live cells, we can write

$$\frac{1}{r}\frac{\partial}{\partial r}\left(r\frac{\partial\sigma}{\partial r}\right) = f(\sigma)\big(v_P + v_Q + v^\dagger\big), \tag{15}$$

where $f(\sigma)$ is the ratio of the consumption rate per unit volume of live cells to the diffusion coefficient. We require $f(\sigma_N) > 0$. At the inner boundary $r = r_0$, i.e. at the vessel wall, we have prescribed the constant oxygen blood concentration $\sigma_b > \sigma_P$,

$$\sigma(r_0,t) = \sigma_b.$$

In the absence of necrosis, the symmetry of vascularization implies that there is no flux of oxygen across the boundary $r = B$. Therefore, we must impose the boundary condition

$$\left.\frac{\partial \sigma}{\partial r}\right|_{r=B(t)} = 0. \tag{16}$$

From the assumption that vessels move solidly with the tissue we have the following equation for $B(t)$:

$$\dot{B} = u\big(B(t), t\big),$$

with the initial condition $B = B_0$.

In the presence of surrounding necrosis, the cord/necrosis interface $r = \rho_N(t)$ is a free boundary of the domain in which oxygen diffusion occurs. This boundary can be determined by noting that the necrotic material cannot be converted to living cells and that assumption (iv) forbids to have living cells for $\sigma < \sigma_N$. Thus, the following inequalities must be satisfied:

$$u\big(\rho_N(t), t\big) - \dot{\rho}_N(t) \geq 0, \tag{17}$$

$$\sigma\big(\rho_N(t), t\big) \geq \sigma_N, \tag{18}$$

together with the no-flux condition

$$\left.\frac{\partial \sigma}{\partial r}\right|_{r=\rho_N(t)} = 0. \tag{19}$$

Therefore, if the cells cross the interface $\rho_N(t)$, i.e. if $u(\rho_N, t) - \dot{\rho}_N > 0$, the cord radius ρ_N is defined by

$$\sigma\big(\rho_N(t), t\big) = \sigma_N,$$

and the interface is a non-material free boundary. Otherwise, as (17) imposes, the cord boundary becomes a material free boundary carrying the condition (19) and its motion is given by

$$\dot{\rho}_N = u\big(\rho_N(t), t\big),$$

whereas $\sigma(\rho_N(t), t)$ can be greater than σ_N. In the presence of necrosis and in the absence of treatment, the cord model admits a stationary state (see Bertuzzi et al., 2007). In this stationary state the (constant) interface ρ_N is always a non-material boundary. Switching to the material boundary may occur during the treatment. This boundary is however subject to the constraint (18), so that if during the cord repopulation $\sigma(\rho_N(t), t)$ tends to drop below σ_N, the free boundary must become non-material again (Bertuzzi et al., 2004).

4. Numerical results

4.1. Single-dose response

To analyze the response to a single dose of radiation, we first simulated the response of a growing cord in the absence of necrosis (as in Fig. 1A). The state of the cord at the time

of irradiation was obtained by allowing the cord to evolve from an initial condition with small B ($B_0 = 30\,\mu$m), $\nu_P = \nu^* = 0.85$, and $\nu_Q = 0$ up to a prefixed radius B. In all the simulations that follow, we assumed $r_0 = 20\,\mu$m and the function $f(\sigma)$ in Eq. (15) of the form

$$f(\sigma) = F\frac{\sigma}{K+\sigma},$$

with $F = 0.016$ mmHg/μm^2 and $K = 4.32$ mmHg (Casciari et al., 1992). Moreover, we chose the following parameter values (O_2 concentration in mmHg and time in h): $\lambda_{\min} = \gamma_{\min} = 0$, $\gamma_{\max}/\chi = \lambda_{\max}/\chi = 1$, $\chi = \log 2/24$, $\sigma_b = 40$, $\sigma_P = 15$, $\sigma_Q = 1.125$, $\sigma_N = 0.5$. The unperturbed growth of the cord with the above set of parameters leads to a stationary state with cord/necrosis interface $\rho_N = 125\,\mu$m, in agreement with the measurements of cord radius by Moore et al. (1984).

The dependence of the radiosensitivity parameters on the oxygen concentration was taken as in Wouters and Brown (1997), with the functions $\psi_\alpha(\sigma)$ and $\psi_\beta(\sigma)$ in Eqs. (13) and (14) having the form

$$\psi_\alpha(\sigma) = \frac{1}{2.5}\,\frac{2.5(\sigma-\sigma_N)+3.28}{\sigma-\sigma_N+3.28},$$

$$\psi_\beta(\sigma) = \frac{1}{3}\,\frac{3(\sigma-\sigma_N)+3.28}{\sigma-\sigma_N+3.28}.$$

In the simulations that follow we have assumed equal radiosensitivity for P and Q cells, i.e. $\alpha_M^P = \alpha_M^Q = \alpha_M$ and $\beta_M^P = \beta_M^Q = \beta_M$.

Figure 3 shows a typical response to a single dose. Panel A reports the volumes (per unit cord length) of the different subpopulations of living cells normalized to the volume of viable cells immediately before the irradiation time, $t = 0$. By defining

$$P(t) = \int_{r_0}^{B(t)} r\nu_P(r,t)\,dr, \qquad Q(t) = \int_{r_0}^{B(t)} r\nu_Q(r,t)\,dr,$$

e.g. in the case of the proliferating viable cells, we have plotted the quantity $P(t)/[P(0^-) + Q(0^-)]$. Before irradiation, the volume fraction of proliferating cells in the whole cord is 86.5%. Following the instantaneous drop caused by the direct action of radiation, there is a further decrease of viable cells due to the misrepair process. When the repair process is virtually completed, the viable (P + Q) cells exhibit a minimum at about 2 h ($= 4/\omega$). The decrease of the live cells is instead slower, and their minimum is delayed according to the death rate constant μ of the lethally damaged cells. This population, which is dominant in the present case during the first stage, becomes practically extinct after about 48 h, as shown by the confluence of the curves representing live cells and P + Q viable cells. The decrement in the amount of live cells reduces oxygen consumption and thus causes a general reoxygenation of the cord, as shown by the time course of mean oxygen concentration and of the oxygen concentration at the boundary B (panel B). These profiles are in a qualitative agreement with the measured oxygen concentrations reported in Crokart et al. (2005).

The reoxygenation shown by panel B produces a transient increment in average radiosensitivity above the pretreatment value. Panel D shows the equivalent α and β values

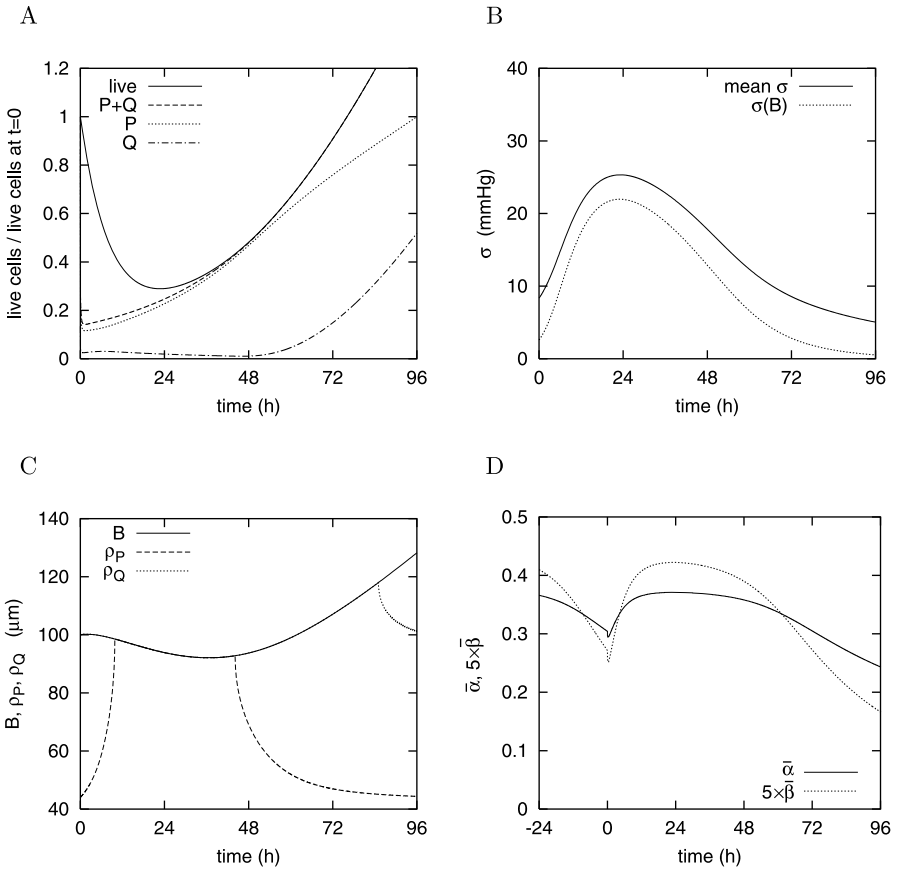

Fig. 3 Single-dose response: time course of live cells and viable subpopulations (panel A), mean oxygen concentration (B), cord radius (C), and equivalent radiosensitivities (D). The difference between live cells and viable P + Q cells in panel A represents the time course of lethally damaged cells. Parameter values: $D = 4\,\mathrm{Gy}$, $\alpha_M = 0.4\,\mathrm{Gy}^{-1}$, $\beta_M = 0.1\,\mathrm{Gy}^{-2}$, $\omega = 2\,\mathrm{h}^{-1}$, $k = 2 \times 10^{-4}\,\mathrm{h}^{-1}$, $\mu = 0.25\,\mathrm{h}^{-1}$, $\mu_N = 0.02\,\mathrm{h}^{-1}$, $B(0) = 100\,\mu\mathrm{m}$.

$\bar{\alpha}$ and $\bar{\beta}$ that characterize the overall sensitivity of the viable cell population in the cord (see Appendix C). These parameters synthetically define the radiobiological status of a cell population with heterogeneous radiosensitivity (Brenner et al., 1995) and are computed here for the cell population in the heterogeneous microenvironment of the tumour cord. The time course of $\bar{\alpha}$ and $\bar{\beta}$ is reported starting 24 h before irradiation. Before irradiation, the average radiosensitivities decrease, because the cord expansion reduces the mean oxygenation of the cells. Immediately after irradiation, a slight instantaneous increase of radioresistance occurs because of the preferential sparing of less oxygenated cells. Thereafter, the radiosensitivity increases due to the reoxygenation process. Panel C reports the time evolution of the cord radius B that shows an initial cord regression followed by regrowth. The decrement of cord radius contributes to the increase in oxygen

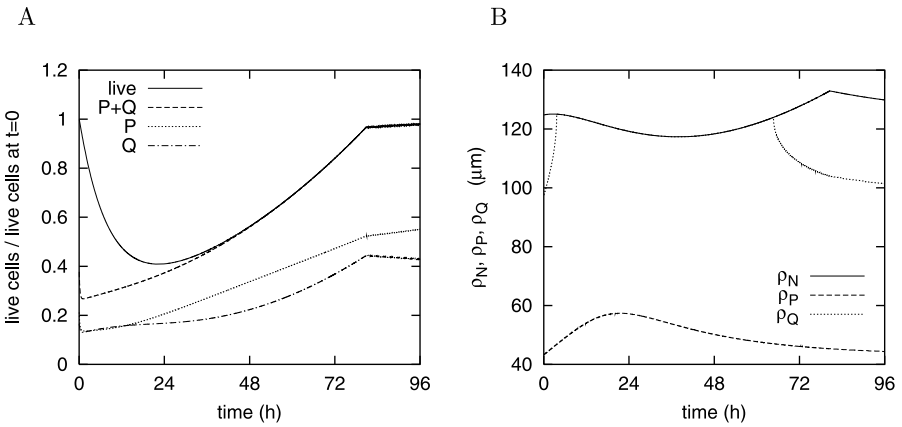

Fig. 4 Single-dose response of a cord surrounded by necrosis: time course of live cells and viable subpopulations (panel A) and cord radius (B). Parameter values as in Fig. 3. At $t = 0$ the cord is at the steady state.

concentration because of the boundary condition (16). The panel also shows the time course of the radii ρ_P and ρ_Q where oxygen concentration is equal to σ_P and, respectively, σ_Q. During cord regrowth the radius B increases beyond the value at $t = 0$, which allows the normalized volume of viable cells to attain later values larger than 1, as shown in panel A. The simulation was stopped before the appearance of the necrotic region.

In the presence of necrosis, the response of the cord to a single dose is qualitatively similar to that illustrated in Fig. 3. However, some differences may be found as shown in Fig. 4. Figure 4 displays the response to irradiation of a cord initially in the stationary state that occurs in the absence of treatment. The cord/necrosis interface, plotted in panel B, shows that the regrowth occurring after the initial shrinkage is interrupted when the interface switches from material to non-material. This event is indicated by the corner point of the curve. Thereafter, the interface tends to the steady-state value and the volume of live cells in panel A eventually tends to the initial value. Note that the time course of the volume of P and Q cells differs from that in Fig. 3A because the initial values of the proliferating and quiescent cell fractions are in this case about the same.

4.2. Split-dose response

After the radiation dose, as seen in panel D of Fig. 3, a transient increase in the radiosensitivity of cells occurs in the cord because of the reoxygenation. The reoxygenation is thus expected to affect the split-dose response modifying the response beyond the prediction of Eq. (5) that only incorporates the effect of repair.

We have compared the response to a single dose D, given at time $t = 0$, with the response to two doses $D/2$ delivered with a time interval T. Figure 5 reports an example of the time course of viable cells in the two cases, with T chosen equal to 36 h. The comparison has been made by computing the survival ratio

$$\mathrm{SR} = \frac{\min[P_2(t) + Q_2(t)]}{\min[P_1(t) + Q_1(t)]},$$

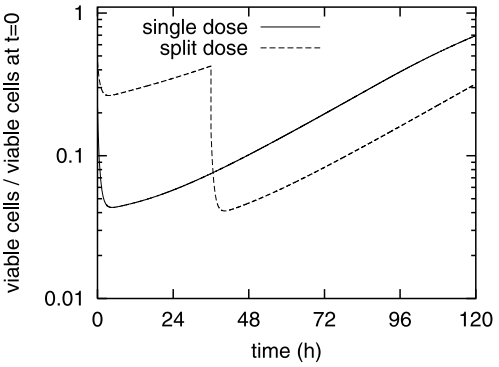

Fig. 5 Example of the cord response (time course of viable P + Q cells) to a single 8 Gy dose compared with the split-dose response with $T = 36$ h. Cord surrounded by necrosis.

where the subscripts 1 , 2 refer to the single-dose response and to the split-dose response, respectively. We recall that the survival ratio predicted by the LQ model is obtained by dividing the surviving fraction of Eq. (5) by the surviving fraction of Eq. (3), which yields

$$\mathrm{SR} = \exp\left[\beta\left(1 - \mathrm{e}^{-\omega T}\right)\frac{D^2}{2}\right]. \tag{20}$$

Note that the SR given by (20) is equal to 1 for $T = 0$ and tends to the constant value $\exp(\beta D^2/2)$ for T large enough to allow the completion of the repair process. The fact that the survival ratio (20) is larger than 1 for $T > 0$ indicates that, according to the LQ model, the dose fractionation always produces the sparing of the cell population.

Figure 6, panel A, shows the behavior of the survival ratio predicted by our model as a function of the interfraction interval T (closed symbols). We note preliminarily that the inclusion in the model of a non-instantaneous repair process implies that the SR curve is equal to unity as T approaches zero, as it is physically reasonable. The initial rising branch of the curve corresponds to the repair process, whose duration is proportional to $1/\omega$. The increase for large T is due to the regrowth of surviving cells in the time interval between the two doses. In coincidence with the time window of increased radiosensitivity, the SR decreases and attains a relative minimum. As a comparison, the open symbols represent the SR computed by a simulation in which the parameters α and β were taken independent of σ and equal to the equivalent values, $\bar{\alpha}$ and $\bar{\beta}$, in the cord before irradiation ($\bar{\alpha} = 0.304\,\mathrm{Gy}^{-1}$ and $\bar{\beta} = 0.054\,\mathrm{Gy}^{-2}$). Except for the steady SR increase due to the regrowth in the interfraction interval, the SR pattern in this case approximately follows Eq. (20). It is thus quite evident that reoxygenation makes the second dose more effective.

Panel B of Fig. 6 shows the effects of changes in the intrinsic radiosensitivities that increase the pretreatment $\bar{\alpha}/\bar{\beta}$ ratio from 5.6, as in panel A, to about 10. The increased $\bar{\alpha}/\bar{\beta}$ is obtained either by increasing α_M or by decreasing β_M. When α_M is increased (open circles) with respect to the reference value (closed circles), the SR curve shows a pronounced lowering of the minimum, due to the stronger reoxygenation caused by increased cell death after the first dose. Thus, unlike the LQ model, the present model predicts that the SR curve also depends on the parameter α. The maximum is less affected, in agreement with the LQ model which predicts that the maximum of survival

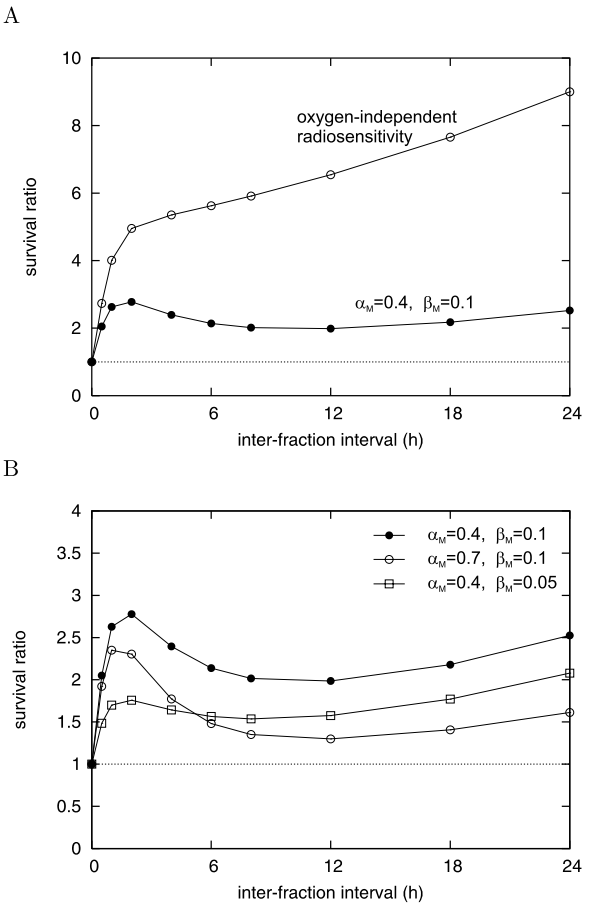

Fig. 6 Survival ratio predicted by the cord model with $B(0) = 100\,\mu\text{m}$, $D = 8\,\text{Gy}$, $\mu = 0.125\,\text{h}^{-1}$, other parameters as in Fig. 3. Panel A. Closed symbols: $\alpha_M = 0.4\,\text{Gy}^{-1}$, $\beta_M = 0.1\,\text{Gy}^{-2}$. Equivalent radiosensitivities at $t = 0^-$: $\bar{\alpha} = 0.304\,\text{Gy}^{-1}$, $\bar{\beta} = 0.054\,\text{Gy}^{-2}$. Open symbols: SR predicted with α and β independent of σ and equal to $\bar{\alpha}$ and $\bar{\beta}$. Panel B: SR for different values of α_M (Gy^{-1}) and β_M (Gy^{-2}) with $\bar{\alpha}/\bar{\beta}$ constant. Closed circles, $\alpha_M = 0.4$ and $\beta_M = 0.1$ (reference curve); open circles, $\alpha_M = 0.7$ and $\beta_M = 0.1$; open squares, $\alpha_M = 0.4$ and $\beta_M = 0.05$.

ratio depends only on β (see Eq. (20)). Conversely, when β_M is decreased (open squares), the whole SR curve is lowered with respect to the reference curve, as it is also expected from Eq. (20). Moreover, the curvature is milder because of the reduced reoxygenation.

Figure 7, panel A, shows the effect of changes in the repair rate ω. The decrease in ω, besides affecting the rising branch of the curve as expected, also produces a decrease in the SR values at large interfraction intervals. Panel B shows the pattern of the survival ratio for different intervessel distances. The split-dose response of the cord was simulated for three different values of B at $t = 0$. In addition, the response of a cord surrounded by necrosis was also simulated. When B increases, the whole SR curve is lowered and

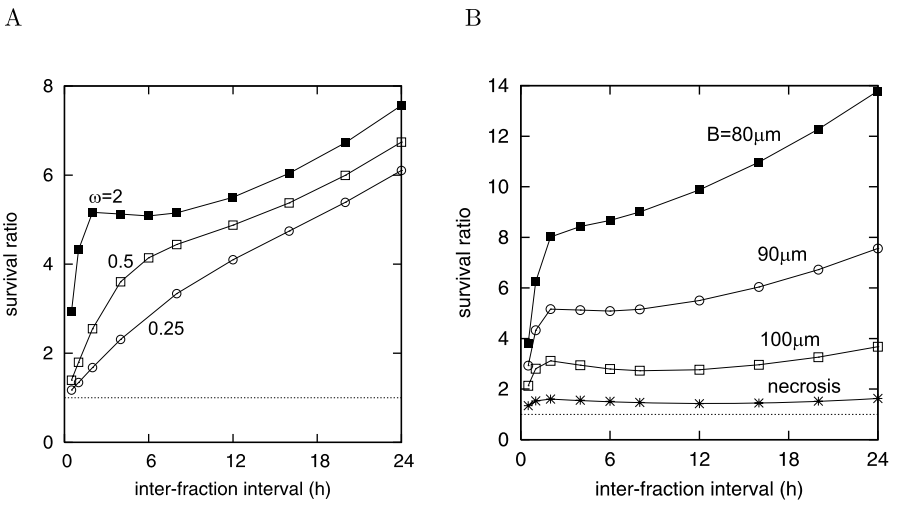

Fig. 7 Panel A: effect of the repair rate on the survival ratio. Closed squares, $\omega = 2\,\mathrm{h}^{-1}$; open squares, $\omega = 0.5\,\mathrm{h}^{-1}$; open circles, $\omega = 0.25\,\mathrm{h}^{-1}$. $B(0) = 90\,\mu\mathrm{m}$, $D = 8\,\mathrm{Gy}$, $\alpha_M = 0.192\,\mathrm{Gy}^{-1}$, $\beta_M = 0.096\,\mathrm{Gy}^{-2}$, $\mu = 0.125\,\mathrm{h}^{-1}$, other parameters as in Fig. 3. Panel B: Effect of the intervessel distance on the survival ratio. Closed squares, $B(0) = 80\,\mu\mathrm{m}$; open circles, $B(0) = 90\,\mu\mathrm{m}$; open squares, $B(0) = 100\,\mu\mathrm{m}$; stars, SR when necrosis occurs ($\rho_N = 125\,\mu\mathrm{m}$). $\omega = 2\,\mathrm{h}^{-1}$, other parameters as in panel A.

reaches a minimum in the case of necrosis, a behavior explained by considering that the mean oxygen concentration decreases and therefore the average β value also decreases. Moreover, if the cord radius is small, the reoxygenation induces only a small increase in radiosensitivity because the initial mean oxygen concentration is high and then the σ values fall in the saturating portion of the $\alpha(\sigma)$ and $\beta(\sigma)$ curves (see equations of ψ_α and ψ_β).

4.3. Split-dose response in tumour and normal tissue

The LQ model allows comparison of the effects of the split-dose delivery in the tumour and in the surrounding normal tissue. By using the LQ model extended to take into account both repair and cell repopulation (Brenner et al., 1995), the surviving fraction after two half-doses is given by

$$S = \exp\left[-\alpha D - \beta\left(1 + \mathrm{e}^{-\omega T}\right)\frac{D^2}{2} + T/\tau_p\right], \tag{21}$$

where τ_p is the time constant of tumour cell repopulation. Similarly, for the surviving fraction of the normal population we have

$$S' = \exp\left[-\alpha' D - \beta'\left(1 + \mathrm{e}^{-\omega' T}\right)\frac{D^2}{2} + T/\tau'_p\right]. \tag{22}$$

To maximize the effect of irradiation on the tumour, we may use the maximal dose which is compatible with an assigned level of damage to normal tissue. Let S_n^* be the

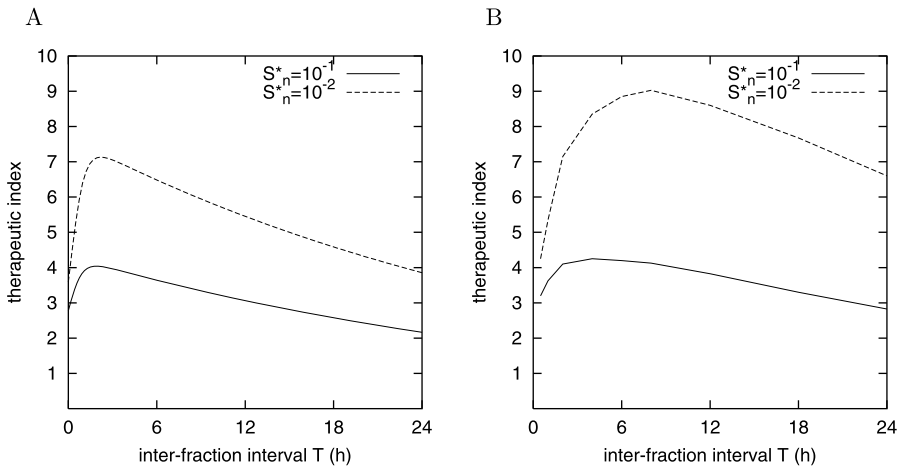

Fig. 8 Panel A. Therapeutic index I for the two-fraction treatment, as predicted by the extended LQ model for two different values of S_n^*. Tumour: $\alpha = 0.5\,\mathrm{Gy}^{-1}$, $\beta = 0.05\,\mathrm{Gy}^{-2}$, $\omega = 2\,\mathrm{h}^{-1}$, $\tau_P = 24\,\mathrm{h}$. Normal tissue: $\alpha' = 0.2\,\mathrm{Gy}^{-1}$, $\beta' = 0.067\ \mathrm{Gy}^{-2}$, $\omega' = 2\,\mathrm{h}^{-1}$, $1/\tau'_P = 0$. Panel B. Therapeutic index I computed by using the cord model for the tumour. Tumour: $\alpha_M = 0.6\,\mathrm{Gy}^{-1}$, $\beta_M = 0.075\,\mathrm{Gy}^{-2}$, $\omega = 2\,\mathrm{h}^{-1}$, $\chi = (\ln 2)/24\,\mathrm{h}^{-1}$, $\mu = 0.125\,\mathrm{h}^{-1}$, $B(0) = 90\,\mu\mathrm{m}$, other parameters as in Fig. 3. Normal tissue, parameters as in panel A.

minimal surviving fraction that may be accepted for normal tissue. From Eq. (22) we can compute for each T the dose $D^*(S_n^*, T)$ that produces a survival $S' = S_n^*$. Then, by substituting this dose D^* in Eq. (21), we obtain the survival of tumour cells, S_t^*, which is compatible with the assigned damage to normal cells. A "therapeutic index" may be defined as $I = S_n^*/S_t^*$.

Figure 8A shows an example of the behavior of the therapeutic index I as a function of the interfraction interval T for given values of the parameters in (21), (22) and two different values of S_n^*. The index I reaches a maximum as the repair process is completed and then decreases with T since the regrowth of the tumour after the first dose is assumed faster than the regrowth of normal tissue. When the required S_n^* is higher, the dose D^* which may be administered will be smaller, and then I will also be smaller. The possibility of having $I > 1$ relies on the difference in the α and β values between the tumour and the normal tissue. From Eqs. (21) and (22) it is easy to see that if $\alpha/\beta > \alpha'/\beta'$, $\tau_p < \tau'_p$, and $\omega' \leq \omega$, then $\alpha > \alpha'$ is a necessary condition to have $I > 1$.

The above analysis disregarded the effect of reoxygenation that may be accounted for by using the tumour cord model. As an example, the tumour may be represented as an array of cords of radius $B = 90\,\mu\mathrm{m}$ (in the absence of necrosis), with α_M and β_M such that the pretreatment $\bar{\alpha}$ and $\bar{\beta}$ values are approximately equal to the values of α and β chosen in Fig. 8A. Moreover, χ may be chosen equal to $\ln 2/\tau_p$, with τ_p as in Fig. 8A, and similarly for ω. A cord representation might also be used for the normal tissue. However, because of the uniformly high oxygenation level in normal tissue due to the small intercapillary distances, the reoxygenation occurring after the first irradiation should not significantly increase the apparent values of the radiosensitivity coefficients. Therefore, in our simulations, we have used the LQ model (22) with constant parameters

for the surviving fraction of normal tissue. Moreover, we have assumed $\omega' = \omega$ and no proliferation of normal tissue.

Figure 8B depicts the therapeutic index as a function of T, computed as described above. The comparison of Figs. 7A and 7B shows that the reoxygenation increases the therapeutic index, in particular at T values much larger than the time when repair is completed.

5. Concluding remarks

In the present study we have proposed a mathematical model for the tumour response to impulsive irradiations. The model assumes an ideal Krogh-type geometry of vascularization and explicitly describes the oxygenation status of tumour cells. Model simulations, using reasonable parameter values in agreement with data from experimental tumours, have shown that substantial reoxygenation may occur after doses of 4 Gy or greater, even if the decrease in oxygen consumption due to treatment-induced cell death is the only cause of reoxygenation. This reoxygenation, whose maximum after a single dose is reached at a time depending on the death rate of lethally damaged cells, appears to reduce the sparing effect of dose fractionation. The model also predicts that the sparing effect of fractionation is remarkably modulated by the intervessel distance. A complex pattern of behaviors of the survival ratio, when the parameter values are changed, has been found in the case of the split-dose response. Values of the survival ratio smaller than 1 were also achieved in the case of cord surrounded by necrosis (data not shown).

The prediction of the reoxygenation time course might be useful in determining the optimal time for delivering the subsequent doses. We must stress, however, that our model assumes that vessels are not affected by the treatment, and thus its application is restricted to the analysis of short sequences of irradiations.

Unlike the extended LQ model proposed by Brenner et al. (1995), in which the resensitization after the first dose only recovers the pretreatment value, the present model predicts that radiosensitivities greater than the pretreatment value can be transiently achieved.

The model could be extended in several directions. The increase in blood perfusion, which has been recognized in some cases to be an important cause of reoxygenation (Sonveaux et al., 2002; Crokart et al., 2005), might be incorporated in the model by a modulation of the oxygen concentration in blood. Moreover, suitable modifications could account for more detailed mechanisms of lethal damage induction and death of damaged cells (Obaturov et al., 1993; Sachs et al., 1997). Finally, we note that our model takes into account the processes of repair, reoxygenation, repopulation and redistribution between proliferating and quiescent cells. To take fully into account the redistribution of cells among the cell cycle phases after irradiation, a more complex, although feasible model should be devised. This model should incorporate a partition of cells into the cell cycle compartments to account for the different phase-specific sensitivities of the cells (Dionysiou et al., 2004; Ribba et al., 2006).

Acknowledgement

This work was partially supported by the FIRB-MIUR Project "Metodi dell'Analisi Matematica in Biologia, Medicina e Ambiente".

Appendix A

In this appendix we show that the model (1), (2), in the case of an impulsive dose D, predicts the expression (3) for the surviving fraction if $2k\delta D/\omega \ll 1$. Let the dose D be given at $t = 0$. Equations (1), (2) rewrite as

$$\frac{dN}{dt} = -\frac{1}{2}kU^2N,$$
$$\frac{dU}{dt} = -\omega U - 2kU^2,$$

with the initial conditions

$$N(0^+) = N(0^-)\exp(-\alpha D),$$
$$U(0^+) = U(0^-) + \delta D, \qquad U(0^-) = 0.$$

The solution of the above system for $t > 0$ may be written as

$$U(t) = \frac{\omega\delta D\mathrm{e}^{-\omega t}}{\omega + 2k\delta D(1-\mathrm{e}^{-\omega t})},$$
$$\log\frac{N(t)}{N(0^+)} = \frac{\omega}{8k}\left(\log\left[1+\frac{2k\delta D}{\omega}\left(1-\mathrm{e}^{-\omega t}\right)\right] - \frac{2k\delta D}{\omega}\,\frac{(\omega+2k\delta D)(1-\mathrm{e}^{-\omega t})}{\omega+2k\delta D(1-\mathrm{e}^{-\omega t})}\right).$$

The latter equation, in the limit $t \to \infty$, provides the surviving fraction $S = \lim_{t\to\infty} N(t)/N(0^-)$ as

$$\log S = -\alpha D + \frac{\omega}{8k}\left(\log\left[1+\frac{2k\delta D}{\omega}\right] - \frac{2k\delta D}{\omega}\right). \tag{A.1}$$

For $2k\delta D/\omega \ll 1$, which corresponds to neglecting the quadratic term in (2), the 2nd-order approximation of the second term in the r.h.s. of (A.1) is $-k\delta^2D^2/(4\omega)$, so that

$$S = \exp\left[-\alpha D - \beta D^2\right],$$

with β given by (4).

Appendix B

We observe preliminarily that Eq. (2) of the model by Hlatky et al. (1994) can be reformulated in terms of the mean DSB density in the cell nucleus, $x = U/V$, where V denotes the volume of cell nucleus. In the case of an impulsive irradiation at time $t = 0$, from Eq. (2) we obtain

$$\frac{dx}{dt} = -\omega x - 2\tilde{k}x^2, \qquad x\left(0^+\right) = \tilde{\delta}D + x(0^-),$$

where $\tilde{k} = Vk$ and $\tilde{\delta} = \delta/V$.

Let us now consider the cord cell population. According to the continuum approach, we may define the density of P-cell DSBs, $x_P(r,t)$, as the function such that $x_P(r,t)\theta v_P(r,t)2\pi r\,dr$ gives their number in the annular region between r and $r+dr$ per unit cord length at time t. Here, θ represents the fraction of cell volume occupied by the nucleus, and it is assumed constant. Similarly, we can define the density of Q-cell DSBs, $x_Q(r,t)$. Writing the balance of double strand breaks in the elementary volume between r and $r+dr$, we obtain

$$\frac{\partial}{\partial t}(x_P v_P)+\frac{1}{r}\frac{\partial}{\partial r}(rux_P v_P)=\gamma x_Q v_Q-\lambda x_P v_P-m_P x_P v_P-\omega x_P v_P-2\tilde{k}x_P^2 v_P,$$

$$\frac{\partial}{\partial t}(x_Q v_Q)+\frac{1}{r}\frac{\partial}{\partial r}(rux_Q v_Q)=-\gamma x_Q v_Q+\lambda x_P v_P-m_Q x_Q v_Q - \omega x_Q v_Q-2\tilde{k}x_Q^2 v_Q.$$

Taking into account Eqs. (6), (7), the above equations become

$$\frac{\partial x_P}{\partial t}+u\frac{\partial x_P}{\partial r}=-\chi x_P+\gamma\frac{v_Q}{v_P}(x_Q-x_P)-\omega x_P-2\tilde{k}x_P^2,$$

$$\frac{\partial x_Q}{\partial t}+u\frac{\partial x_Q}{\partial r}=\lambda\frac{v_P}{v_Q}(x_P-x_Q)-\omega x_Q-2\tilde{k}x_Q^2.$$

Since the repair/misrepair process is in general very fast, we can disregard the terms in χ, γ and λ. Thus, we have

$$\frac{\partial x_P}{\partial t}+u\frac{\partial x_P}{\partial r}=-\omega x_P-2\tilde{k}x_P^2, \tag{B.1}$$

$$\frac{\partial x_Q}{\partial t}+u\frac{\partial x_Q}{\partial r}=-\omega x_Q-2\tilde{k}x_Q^2. \tag{B.2}$$

Defining

$$X_P(r,t)=Vx_P(r,t),\qquad X_Q(r,t)=Vx_Q(r,t),$$

we can rewrite (B.1) and (B.2) getting Eqs. (11), (12). Note that X_P $[X_Q]$ can be interpreted as the number of double strand breaks in an "equivalent" cell having a uniform DSB concentration x_P $[x_Q]$ in its nucleus.

Appendix C

The radiosensitivity of the cell population in the cord can be traced at any time t by considering the fraction of cells expected to survive, after the delivery of an impulsive dose D at that time, according to the LQ model (with instantaneous repair). This survival, $S(t,D)$, can be expressed as

$$S(t,D)=\frac{\int_{r_0}^{B(t)} r[v_P(r,t)s_P(r,t)+v_Q(r,t)s_Q(r,t)]\,dr}{\int_{r_0}^{B(t)} r[v_P(r,t)+v_Q(r,t)]\,dr}, \tag{C.1}$$

with

$$s_P(r,t) = \exp\bigl[-\alpha_P\bigl(\sigma(r,t)\bigr)D - \beta_P\bigl(\sigma(r,t)\bigr)D^2\bigr], \tag{C.2}$$

$$s_Q(r,t) = \exp\bigl[-\alpha_Q\bigl(\sigma(r,t)\bigr)D - \beta_Q\bigl(\sigma(r,t)\bigr)D^2\bigr]. \tag{C.3}$$

We define as "equivalent radiosensitivities" the quantities $\bar{\alpha}(t)$ and $\bar{\beta}(t)$ such that

$$S(t) \simeq \exp\bigl[-\bar{\alpha}(t)D - \bar{\beta}(t)D^2\bigr]. \tag{C.4}$$

Considering the second-order expansion of $\ln S(t, D)$ about $D = 0$, we obtain

$$\ln S(t) \simeq -\langle\alpha\rangle(t)D - \frac{1}{2}\bigl(2\langle\beta\rangle(t) - \langle\alpha^2\rangle(t) + \langle\alpha\rangle^2(t)\bigr)D^2,$$

where

$$\langle\alpha\rangle(t) = \frac{\int_{r_0}^{B(t)} r[v_P(r,t)\alpha_P(\sigma(r,t)) + v_Q(r,t)\alpha_Q(\sigma(r,t))]\,dr}{\int_{r_0}^{B(t)} r[v_P(r,t) + v_Q(r,t)]\,dr},$$

and $\langle\beta\rangle$, $\langle\alpha^2\rangle$ are averages similarly defined. If we define

$$\bar{\alpha} = \langle\alpha\rangle,$$

$$\bar{\beta} = \langle\beta\rangle - \frac{1}{2}\bigl(\langle\alpha^2\rangle - \langle\alpha\rangle^2\bigr) = \langle\beta\rangle - \frac{1}{2}\mathrm{Var}(\alpha),$$

we get Eq. (C.4).

We note that the third-order term of the expansion of $\ln S$ is given by

$$\frac{1}{6}\bigl(-\langle\alpha^3\rangle - 2\langle\alpha\rangle^3 + 3\langle\alpha\rangle\langle\alpha^2\rangle + 6\langle\alpha\beta\rangle - 6\langle\alpha\rangle\langle\beta\rangle\bigr)D^3,$$

and therefore its extent is related to the heterogeneity of the coefficients α and β in the cord.

References

Alarcón, T., Byrne, H.M., Maini, P.K., 2003. A cellular automaton model for tumour growth in inhomogeneous environment. J. Theor. Biol. 225, 257–274.

Belli, J.A., Dicus, G.J., Bonte, F.J., 1967. Radiation response of mammalian tumor cells. I. Repair of sublethal damage in vivo. J. Natl. Cancer Inst. 38, 673–682.

Bertuzzi, A., d'Onofrio, A., Fasano, A., Gandolfi, A., 2003. Regression and regrowth of tumour cords following single-dose anticancer treatment. Bull. Math. Biol. 65, 903–931.

Bertuzzi, A., Fasano, A., Gandolfi, A., 2004. A free boundary problem with unilateral constraints describing the evolution of a tumour cord under the influence of cell killing agents. SIAM J. Math. Anal. 36, 882–915.

Bertuzzi, A., Fasano, A., Gandolfi, A., Sinisgalli, C., 2007. Cell resensitization after delivery of a cycle-specific anticancer drug and effect of dose splitting: learning from tumour cords. J. Theor. Biol. 244, 388–399.

Brenner, D.J., Hlatky, L.R., Hahnfeldt, P.J., Hall, E.J., Sachs, R.K., 1995. A convenient extension of the linear-quadratic model to include redistribution and reoxygenation. Int. J. Radiat. Oncol. Biol. Phys. 32, 379–390.

Bristow, R.G., Hill, R.P., 1998. Molecular and cellular basis of radiotherapy. In: I.F. Tannock, R.P. Hill (Eds.), The Basic Science of Oncology, pp. 295–321. McGraw–Hill, New York.

Byrne, H.M., Preziosi, L., 2003. Modelling solid tumour growth using the theory of mixtures. Math. Med. Biol. 20, 341–366.

Casciari, J.J., Sotirchos, S.V., Sutherland, R.M., 1992. Variations in tumor cell growth rates and metabolism with oxygen concentration, glucose concentration, and extracellular pH. J. Cell. Physiol. 151, 386–394.

Chapman, J.D., Dougle, D.L., Reuvers, A.P., Meeker, B.E., Borsa, J., 1974. Studies on the radiosensitizing effects of oxygen in Chinese hamster cells. Int. J. Radiat. Biol. 26, 383–389.

Crokart, N., Jordan, B.F., Baudelet, C., Ansiaux, R., Sonveaux, P., Grégoire, V., Beghein, N., DeWever, J., Bouzin, C., Feron, O., Gallez, B., 2005. Early reoxygenation in tumors after irradiation: determining factors and consequences for radiotherapy regimens using daily multiple fractions. Int. J. Radiat. Oncol. Biol. Phys. 63, 901–910.

Curtis, S.B., 1986. Lethal and potentially lethal lesions induced by radiations—a unified repair model. Radiat. Res. 106, 252–270.

Dionysiou, D.D., Stamatakos, G.S., Uzunoglu, N.K., Nikita, K.S., Marioli, A., 2004. A four-dimensional simulation model of tumour response to radiotherapy in vivo: parametric validation considering radiosensitivity, genetic profile and fractionation. J. Theor. Biol. 230, 1–20.

Goda, F., O'Hara, J.A., Rhodes, E.S., Liu, K.J., Dunn, J.F., Bacic, G., Swartz, H.M., 1995. Changes of oxygen tension in experimental tumors after a single dose of X-ray irradiation. Cancer Res. 55, 2249–2252.

Hirst, D.G., Denekamp, J., 1979. Tumour cell proliferation in relation to the vasculature. Cell Tissue Kinet. 12, 31–42.

Hlatky, L.R., Hahnfeldt, P., Sachs, R.K., 1994. Influence of time-dependent stochastic heterogeneity on the radiation response of a cell population. Math. Biosci. 122, 201–220.

Jostes, R.F., Williams, M.E., Barcellos-Hoff, M.H., Hoshino, T., Deen, D.F., 1985. Growth delay in 9L rat brain tumor spheroids after irradiation with single and split doses of X rays. Radiat. Res. 102, 182–189.

Kocher, M., Treuer, H., 1995. Reoxygenation of hypoxic cells by tumor shrinkage during irradiation. A computer simulation. Strahlenter. Onkol. 171, 219–230.

Kocher, M., Treuer, H., Voges, J., Hoevels, M., Sturm, V., Müller, R.-P., 2000. Computer simulation of cytotoxic and vascular effects of radiosurgery in solid and necrotic brain metastases. Radiother. Oncol. 54, 149–156.

Krogh, A., 1919. The number and distribution of capillaries in muscles with calculations of the oxygen pressure head necessary to supply the tissue. J. Physiol. 52, 409–415.

Ljungkvist, A.S.E., Bussink, J., Kaanders, J.H.A.M., Wiedenmann, N.E., Vlasman, R., van der Kogel, A.J., 2006. Dynamics of hypoxia, proliferation and apoptosis after irradiation in a murine tumor model. Radiat. Res. 165, 326–336.

Moore, J.V., Hopkins, H.A., Looney, W.B., 1984. Tumour-cord parameters in two rat hepatomas that differ in their radiobiological oxygenation status. Radiat. Environ. Biophys. 23, 213–222.

Moore, J.V., Hasleton, P.S., Buckley, C.H., 1985. Tumour cords in 52 human bronchial and cervical squamous cell carcinomas: inferences for their cellular kinetics and radiobiology. Br. J. Cancer 51, 407–413.

Obaturov, G.M., Moiseenko, V.V., Filimonov, A.S., 1993. Model of mammalian cell reproductive death. I. Basic assumptions and general equations. Radiat. Environ. Biophys. 32, 285–294.

O'Hara, J.A., Goda, F., Demidenko, E., Swartz, H.M., 1998. Effect on regrowth delay in a murine tumor of scheduling split-dose irradiation based on direct pO2 measurements by electron paramagnetic resonance oximetry. Radiat. Res. 150, 549–556.

Popel, A.S., 1989. Theory of oxygen transport to tissue. Crit. Rev. Biomed. Eng. 17, 257–321.

Ribba, B., Colin, T., Schnell, S., 2006. A multiscale mathematical model of cancer, and its use in analyzing irradiation therapies. Theor. Biol. Med. Model. 3, 7, doi: 10.1186/1742-4682-3-7.

Sachs, R.K., Hahnfeld, P., Brenner, D.J., 1997. The link between low-LET dose-response relations and the underlying kinetics of damage production/repair/misrepair. Int. J. Radiat. Biol. 72, 351–374.

Secomb, T.W., Hsu, R., Dewhirst, M.W., Klitzman, B., Gross, J.F., 1993. Analysis of oxygen transport to tumor tissue by microvascular networks. Int. J. Radiat. Oncol. Biol. Phys. 25, 481–489.

Sonveaux, P., Dessy, C., Brouet, A., Jordan, B.F., Grégoire, V., Gallez, B., Balligard, J.L., Feron, O., 2002. Modulation of the tumor vasculature functionality by ionizing radiation accounts for tumor radiosensitization and promotes gene delivery. FASEB J. 16, 1979–1981.

Tannock, I.F., 1968. The relation between cell proliferation and the vascular system in a transplanted mouse mammary tumour. Br. J. Cancer 22, 258–273.

Thames, H.D., 1985. An 'incomplete-repair' model for survival after fractionated and continuous irradiations. Int. J. Radiat. Biol. 47, 319–339.

Vaupel, P., Frinak, S., O'Hara, M., 1984. Direct measurement of reoxygenation in malignant mammary tumors after a single large dose of irradiation. Adv. Exp. Med. Biol. 180, 773–782.

Wong, C.S., Hill, R.P., 1998. Experimental radiotherapy. In: I.F. Tannock, R.P. Hill (Eds.), The Basic Science of Oncology, pp. 322–349. McGraw–Hill, New York.

Wouters, B.G., Brown, J.M., 1997. Cells at intermediate oxygen levels can be more important than the "hypoxic fraction" in determining tumor response to fractionated radiotherapy. Radiat. Res. 147, 541–550.

Zhao, M., Pipe, J.G., Bonnett, J., Evelhoch, J.L., 1996. Early detection of treatment response by diffusion-weighted ^{1}H-NMR spectroscopy in a murine tumour in vivo. Br. J. Cancer 73, 61–64.